Article

Valorization Potential of Polish Laterite Leaching Residues through Alkali Activation

Vasiliki Karmali [1], Evangelos Petrakis [1], Georgios Bartzas [2] and Konstantinos Komnitsas [1,*]

[1] School of Mineral Resources Engineering, Technical University of Crete, 73100 Chania, Greece
[2] School of Mining and Metallurgical Engineering, National Technical University of Athens, Zografos Campus, 15780 Athens, Greece
[*] Correspondence: komni@mred.tuc.gr; Tel.: +30-28210-37686

Abstract: In this study, the valorization potential of Polish laterite leaching residues through alkali activation with the use of NaOH and Na_2SiO_3 solutions as activators was investigated. The effect of the main factors, namely the H_2O/Na_2O molar ratio in the activating solution, the curing temperature, and the ageing period on the main properties of the produced alkali activated materials (AAMs) was assessed. The experimental results showed that AAMs with sufficient compressive strength were only produced when the laterite leaching residues were mixed with significant quantities of metakaolin; thus, when the mass ratio of laterite leaching residues and metakaolin was 0.50, after curing at 40 °C for 24 h and ageing for 7 days, the produced AAMs acquired compressive strength that slightly exceeded 25 MPa. X-ray diffraction (XRD), Fourier transform infrared (FTIR) spectroscopy, scanning electron microscopy, and energy dispersive X-ray spectroscopy (SEM–EDS) analysis were used for the characterization of the raw materials and selected AAMs. Furthermore, the structural integrity of the specimens was investigated after immersion in distilled water and acidic solution (1 mol L^{-1} HCl), or after firing at higher temperatures. Finally, the toxicity of the produced AAMs was assessed with the use of standard leaching tests.

Keywords: laterite leaching residues; metakaolin; alkali activating materials; compressive strength

1. Introduction

Laterites, which contain elevated concentrations of Ni, Al, Fe and in some cases Co, are formed as a result of the intense weathering of rocks in hot and wet climates [1–4]. They are mainly treated pyrometallurgically for the production of ferronickel (FeNi). On the other hand, several alternative hydrometallurgical techniques have been developed for their treatment, including high-pressure acid leaching (HPAL) [5,6], atmospheric leaching [7–10], and heap leaching [11–13].

Alkali activation involves the dissolution of Si and Al from raw materials with the use of strong alkaline solutions, and aims at the formation of secondary, partially amorphous, three-dimensional aluminosilicates consisting of Si-O-Al bonds, called alkali-activated materials (AAMs) or geopolymers [14]. The best raw materials used for the production of AAMs include pozzolans, kaolin, metakaolin, and various industrial wastes, such as fly ash, bauxite residue (red mud), and various types of slags produced from the steel and the non-ferrous metal industry, as well as construction and demolition wastes [15–22]. The produced AAMs exhibit high compressive strength, strong acid resistance, good thermal stability, low shrinkage, and the tendency to immobilize hazardous elements [23–25]. However, their properties depend on several factors, namely the type and particle size of the raw materials and the type of activator, as well as the synthesis conditions, which mainly include the solids:liquids ratio, the H_2O/Na_2O and the SiO_2/Na_2O molar ratios in the alkali activating solution, and the curing temperature and the ageing period [26–29].

So far, most studies have focused on the production of AAMs with the use of lateritic soils [30–34], while only a few studies explored the alkali activation of laterite leaching

residues, which if disposed of in the environment without specific care, may cause the contamination of soils and water resources [35,36].

The present study investigates the alkali activation potential of the residues obtained after the atmospheric sulfuric acid leaching of Polish laterites in stirred reactors and the characterization of the produced AAMs. The novelty of the study is associated with the valorization of a by-product, considered today as waste, with poor inherent alkali activation potential, for which the only management option is its disposal in landfills for hazardous wastes after pretreatment, which mainly involves the neutralization of its residual acidity. To the best of our knowledge, this is the second study dealing with the valorization of similar by-products; a previous study explored the alkali activation potential of residues obtained after larger scale laboratory column leaching tests of Greek laterites [37].

2. Materials and Methods

2.1. Materials

The materials used in the present study were (i) leaching residues obtained after atmospheric H_2SO_4 leaching of Polish laterites (PLR) in 3 L stirred tank reactors and (ii) metakaolin (MK) produced in the laboratory after the calcination of kaolin [$Al_2Si_2O_5(OH)_4$, Fluka] at 750 °C for 2 h in a laboratory oven (N-8L Selecta, Abrera, Spain).

Metakaolin has pozzolanic properties, increased reactivity and good potential for alkali activation; it was mixed with PLR to regulate the SiO_2/Al_2O_3 ratio in the starting mixture [38]. The selection of the calcination temperature was based on the results of a previous study [37].

The PLR were used as received. The material was washed several times to remove any residual acidity and to avoid partial consumption of the activating solution during alkali activation; thus, the paste pH of the PLR prior to use increased to 5.31. Both the PLR and MK were oven-dried at 80 °C for 24 h to remove any remaining moisture and then pulverized in a Bico-type pulverizer (Fritsch, Dresden, Germany) to decrease their particle size and thus increase their specific surface area and subsequent rate of alkali activation reactions. The grain size distribution of the raw materials was determined using a laser particle size analyzer (Mastersizer S, Malvern Instruments, Malvern, UK). Table 1 presents the d_{90} (90% passing) and d_{50} (50% passing), as well as the specific surface area for both raw materials. The specific surface area of PLR was much higher, due to the acid attack of the laterite ore during leaching, which caused the generation of pores and cracks.

Table 1. The d_{90}, d_{50}, and specific surface area of raw materials.

Particle Size (μm)	d_{90} (μm)	d_{50} (μm)	Specific Surface Area (m²/g)
PLR	13.0	2.3	65.3
MK	25.5	8.8	2.4

Table 2 presents the chemical composition of both raw materials in the form of oxides, as obtained from the use of a Bruker-AXS S2 Range Spectroscopic Fluorescence Spectrometer A (XRF-EDS, Bruker, Karlsruhe, Germany). The loss in ignition (LOI) was determined after heating the raw materials at 1050 °C for 4 h. It was observed that the PLR had a high content of SO_3 (30.6 wt%), which was due to the formation of secondary products during leaching, mainly gypsum ($CaSO_4 \cdot 2H_2O$) and bassanite ($CaSO_4 \cdot 0.5H_2O$), as also shown in Section 3.7.1. The low content of Al_2O_3 (1.2 wt%) denoted poor alkali activation potential of the PLR and thus, the addition of amendments was required for their valorization. On the other hand, the MK had a high content of SiO_2 (54.2 wt%) and Al_2O_3 (40.3 wt%), which indicated high reactivity during alkali activation, as confirmed in earlier studies [37,39].

Table 2. Chemical composition (wt%) of raw materials.

Oxide (%)	PLR	MK
Na_2O	8.1	1.3
Fe_2O_3	9.0	0.6
SiO_2	23.3	52.5
Al_2O_3	1.2	38.6
Cr_2O_3	0.4	0.02
MgO	5.9	0.3
NiO	0.4	-
K_2O	0.01	2.4
TiO_2	0.01	0.4
CoO	0.02	<0.00097
MnO	0.1	0.01
CaO	17.9	0.1
P_2O_5	0.2	0.5
SO_3	30.6	0.1
ZnO	-	<0.00003
LOI *	2.9	3.3
SUM	100.0	100.1

* LOI: Loss in ignition was determined after heating of each material at 1050 °C for 4 h.

2.2. Alkali Activation

The solution used for the alkali activation of the raw materials was a mixture of sodium hydroxide (NaOH) and sodium silicate (Na_2SiO_3). First, NaOH pellets (Sigma Aldrich) were dissolved in distilled water to obtain solutions with different molarities (6–10 mol L^{-1}). The resulting solutions were stirred for 5 min and cooled at ambient temperature. Then they were mixed with sodium silicate solution (8 wt% Na_2O, 27 wt% SiO_2, 65 wt% H_2O, Merck) and left overnight prior to use. The raw materials, PLR and MK, were mixed at mass ratios of 50:50 (PLR50MK50) and 70:30 (PLR70MK30), and the mixtures were then alkali activated. The AAM codes, the mixing proportions, and the values of the main experimental parameters are shown in Table 3. The selection of these ratios was based on preliminary tests and the results of earlier studies dealing with the alkali activation of residues obtained after the heap leaching of Greek laterites for a long period [37]. The mixing went on for 10 min in a laboratory mixer, and the homogeneous paste obtained was poured into metallic cubic molds with dimensions of $5 \times 5 \times 5$ cm^3.

Table 3. Experimental parameters for the synthesis of AAMs.

AAMs Code	Solids (wt%)		NaOH (mol L^{-1})	NaOH (wt%)	$H_{2.5}O$ (wt%)	$Na_{2.5}SiO_3$ (wt%)	L/S Ratio *	H_2O/Na_2O **	SiO_2/Na_2O **
	PLR	MK							
PLR50MK50_1	25.1	25.1	6	4.9	20.0	24.9	0.81	21.4	1
PLR50MK50_2	26.4	26.4	8	5.9	18.2	23.1	0.70	17.3	1
PLR50MK50_3	27.1	27.1	10	7.0	15.9	22.9	0.63	14.6	1
PLR70MK30_1	34.7	14.8	6	5.0	20.3	25.2	0.83	21.4	1
PLR70MK30_2	34.8	14.9	8	6.4	18.7	25.2	0.78	17.3	1
PLR70MK30_3	35.7	15.3	10	7.5	17.0	24.5	0.71	14.6	1

* Liquid-to-solid ratio in the starting mixture, ** molar ratios in the activating solution.

The molds were vibrated for 2 min to remove any trapped air bubbles and kept at room temperature for 4 h to enable initial hardening of the paste and the formation of cubic specimens. After demolding, the specimens were placed in plastic bags to prevent any loss of moisture and placed in an oven (Jeio Tech ON-02G, Seoul, Korea) for curing at various temperatures (40 °C, 60 °C, 80 °C, and 95 °C). After curing for 24 h, the specimens were removed from the oven, cooled down, and left for ageing at ambient temperature for 7 and 28 days.

The thermal response of selected AAMs was evaluated after firing them in a laboratory furnace (N-8L Selecta) at temperatures up to 800 °C. The heating rate used was 5 °C min^{-1},

while the retention time at each temperature was 2 h. Also, selected AAMs were immersed in distilled water (H_2O) and acidic solution (1 mol L^{-1} HCl) for 7 days, in order to assess their structural integrity. After each test, compressive strength (MPa), weight loss (%), and volumetric shrinkage (%) were determined.

2.3. Characterization Method Techniques

The reactivity of raw materials was evaluated through the leaching of 1.0 g of each raw material in 100 mL of 10 mol L^{-1} NaOH. Leaching tests were carried out at ambient temperatures in 250 mL conical flasks under continuous stirring for 24 h. After solid–liquid separation using 0.45 μm pore-sized membrane Chromafil PTFE filters (Macherey-Nagel GmbH and Co., Düren, Germany), the concentration of Al and Si in the leaching solution was determined using an Agilent 7500cx Inductively Coupled Plasma Mass Spectrometer (Agilent Technologies Inc., Santa Clara, CA, USA) equipped with an Agilent ASX-500 Autosampler.

The compressive strength (MPa) of the AAMs was determined after an ageing period of 7 or 28 days, using a Matest type compression and flexural machine (C123N, Matest S.p.A, Treviolo, Bergamo, Italy) with a dual range of 500/15 kN. The density (g cm^{-3}), the porosity (%), and the water absorption (%) of selected AAMs were evaluated according to BS EN 1936:2006 [40]. The mean values of each parameter, obtained after three measurements, were used in the following sections.

The mineralogical analysis of the raw materials and selected AAMs was performed with the use of an X-ray diffractometer (XRD) (Bruker AXS (D8 Advance type), Karlsruhe, Germany) (Cu tube, scanning range 4° to 70° at 2θ, step 0.02° and measuring time 0.2 s/step). Qualitative analysis was carried out with the use of DiffracPlus software (EVA v. 2006, Bruker, Karlsruhe, Germany) and the Powder Diffraction File (PDF-2) database. The functional groups of the raw materials and selected AAMs were determined by Fourier Transform Infrared (FTIR) spectroscopy, using pellets and a PerkinElmer 1000 spectrometer (PerkinElmer, Akron, OH, USA), in the spectra range of 400 to 4000 cm^{-1}. Pellets were produced by mixing each powdered material with KBr at a ratio of 1:100 *w/w*, and then the mixture was pressed to obtain a pellet.

Microstructural analysis was performed with the use of scanning electron microscopy (SEM) and energy dispersive X-ray spectroscopy (EDS). For that purpose, a JEOL–6380LV scanning microscope (JEOL Ltd., Tokyo, Japan), operating at an accelerating voltage of 20 kV equipped with an Oxford INCA EDS microanalysis system (Oxford Instruments, Abingdon, UK), was used.

The toxicity of raw materials and selected AAMs was determined with the use of the standard leaching procedure [41,42]. The test involved the leaching of raw material or selected AAMs in distilled water (8 L per kg) for 24 h. After leaching, the solution was filtered using 0.45 μm-sized membrane filters, and the concentration of the metal ions in the eluate was determined (in mg kg^{-1} of raw material) and compared with existing limits for the disposal of wastes in various landfill types [43]. The ion concentration in the solution was determined using an Inductively Coupled Plasma Mass Spectrometer (ICP MS, Agilent 7500 cx) equipped with an Agilent ASX-500 Autosampler.

3. Results and Discussion

3.1. Reactivity of Raw Materials in Alkaline Media

The reactivity of the PLR and MK, as indicated by the concentration of Al and Si in the alkaline solution and the respective Si/Al molar ratios, are shown in Table 4. It was observed that the leaching of the PLR resulted in a low concentration of Al (0.5 mg L^{-1}) in the solution and a much higher Si concentration (59.1 mg L^{-1}), while MK leaching resulted, as expected, in high concentrations of both elements (61.3 mg L^{-1} Si and 43.4 mg L^{-1} Al). Thus, the resulting Si/Al molar ratios were 118.2 and 1.4 for the PLR and MK, respectively.

Table 4. Concentration of Si, Al, and Si/Al molar ratios in NaOH solution *.

Raw Material	Si (mg L^{-1})	Al (mg L^{-1})	Si/Al
PLR	59.1	0.5	118.2
MK	61.3	43.4	1.4

* Leaching with 10 mol L^{-1} NaOH solution for 24 h.

3.2. Effect of H$_2$O/Na$_2$O Molar Ratio in the Activating Solution and Ageing Period

The inherent alkali activation potential of the PLR was very low, which was mainly due to the low content of Al$_2$O$_3$ in the raw material and the unfavorable ratio of Si/Al in the solution and resulting reactive paste [44–47]. As a result, the compressive strengths of the produced AAMs did not exceed 2 MPa, as also indicated in a previous study using residues from laboratory column leachings of a different type of Greek laterite [37]. On the other hand, when only MK was used as the raw material, under similar experimental conditions (H$_2$O/Na$_2$O and SiO$_2$/Na$_2$O molar ratios in solution at 14.6 and 1.0 respectively, curing temperature at 40 °C, curing period at 24 h and ageing period at 7 days), the produced AAMs acquired high compressive strengths of 55 MPa.

Figure 1 presents the compressive strengths of the AAMs produced from mixtures of PLR and MK at mass ratios of 50:50 (PLR50MK50, Figure 1a) and 70:30 (PLR70MK30, Figure 1b) as a function of the H$_2$O/Na$_2$O molar ratio (21.4, 17.3, 14.6). It is seen from these results that the effect of the H$_2$O/Na$_2$O molar ratio on the activating solution is very important, as its reduction from 21.4 to 14.6 resulted in a noticeable increase in the compressive strength of the produced AAMs from almost 10 to 25 MPa. On the other hand, longer ageing periods, namely 28 days, had practically no effect on the compressive strength of the produced AAMs, thus indicating that the alkali activating reactions were completed within a few days.
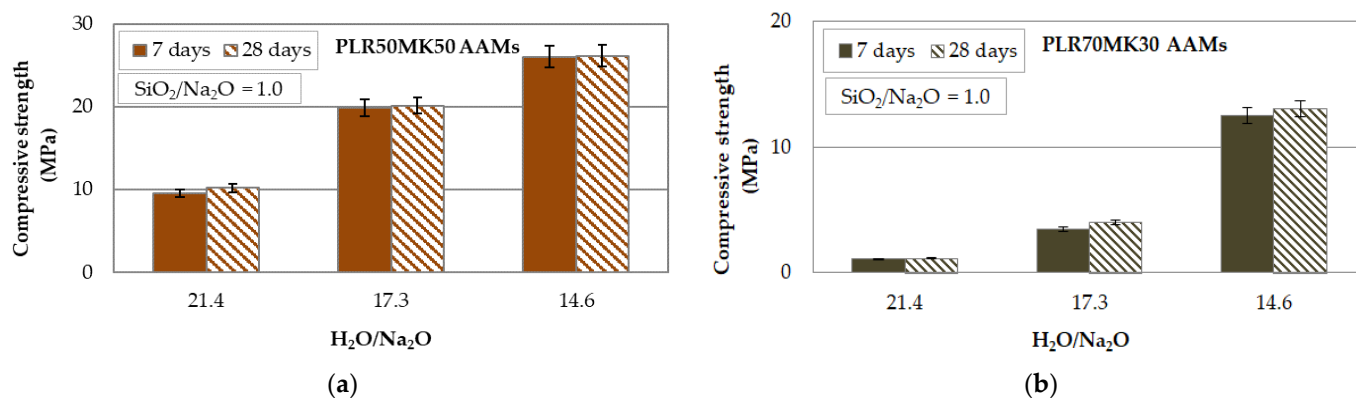

Figure 1. Effect of H$_2$O/Na$_2$O molar ratio on the activating solution and ageing period on the compressive strengths of (**a**) PLR50MK50 and (**b**) PLR70MK30 AAMs (pre-curing time 4 h, curing temperature 40 °C, curing time 24 h; error bars indicate the standard deviation of measurements obtained from three specimens).

It is known that the low molarity of a NaOH solution, i.e., high H$_2$O/Na$_2$O ratio in the solution, results in the deficiency of hydroxyl ions, the limited formation of aluminosilicate bonds, and the low compressive strengths of the produced AAMs. On the other hand, higher molarity, i.e., low a H$_2$O/Na$_2$O ratio in the solution, may indicate an excess of hydroxyl ions in the reactive paste, some of which will remain unreacted, and the produced specimens will acquire low compressive strength. Thus, the optimum H$_2$O/Na$_2$O ratio in each case depends on the raw material type, its reactivity, and ultimately on the reaction rate [48–50].

Also, the experimental results show that the increase of MK content in the starting mixture resulted in the production of AAMs with higher compressive strengths of (PLR50MK50, Figure 1a) up to 26.2 MPa.

3.3. Effect of Curing Temperature and Selected Molar Ratios

The effect of curing temperature on the compressive strengths of PLR50MK50 and PLR70MK30 AAMs is presented in Figure 2. The H_2O/Na_2O and SiO_2/Na_2O molar ratios in the activating solution were 14.6 and 1.0, respectively, while the ageing period was 7 days. As seen from the results, the increase in temperature from 40 to 60 °C had only a minor positive effect on the compressive strengths of the produced AAMs, whereas at higher temperatures, a decrease in the compressive strength was noted.
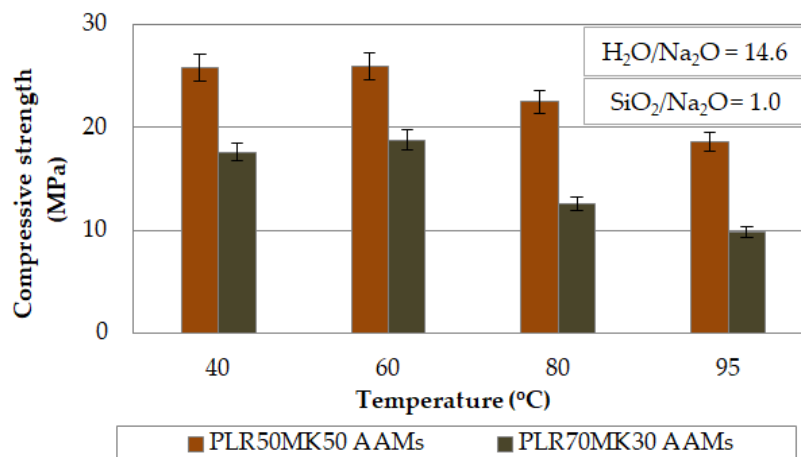

Figure 2. Effect of curing temperature on the compressive strengths of PLR50MK50 and PLR70MK30 AAMs (pre-curing time 4 h, curing time 24 h, ageing period 7 days; error bars indicate the standard deviation of measurements obtained from three specimens).

The compressive strengths obtained after curing at 40 °C were 25.9 and 17.6 MPa for the PLR50MK50 and PLR70MK30 AAMs, respectively. It is known that the increase in curing temperature in most cases increases the rate of the alkali activation reactions and enables the formation of stronger bonds [29]. However, in some cases, curing at high temperature may cause a rapid loss of moisture from the reactive paste, and this results in the development of microcracks and the production of specimens with poor properties [51–56].

Table 5 presents the effect of SiO_2/Al_2O_3 and $(SiO_2 + Al_2O_3)/Na_2O$ molar ratios present in the reactive paste on the compressive strengths of the produced AAMs.

Table 5. Effect of oxide molar ratios in the reactive paste on the compressive strengths of selected AAMs [1].

AAMs Code	Compressive Strength (MPa)	NaOH (M)	SiO_2/Al_2O_3	$(SiO_2 + Al_2O_3)/Na_2O$
PLR50MK50	25.9	10	4.1	3.6
PLR70MK30	17.6		6.0	2.6

[1] H_2O/Na_2O = 14.6, SiO_2/Na_2O = 1.0, curing at 40 °C for 24 h and ageing for 7 days.

Both ratios are very important and indicate the effect of the composition of the reactive phase on alkali activation [57–59]. The optimum ratios during alkali activation differ and mainly depend on the type of the raw material; however, sufficient concentrations of both elements are required so that the produced AAMs acquire adequate compressive strengths [49,60,61]. For example, higher molarities of NaOH, i.e., lower $(SiO_2 + Al_2O_3)/Na_2O$ ratios, may result in the production of AAMs with lower compressive strengths, because part of the alkaline solution may not react. In the present study, the addition of MK resulted in increased reactivity of the precursors and thus higher concentrations of Si and Al ions in the reactive paste, which are required for the development of aluminosilicate bonds. On the other hand, the presence of sulphates and other ions, such as nitrates or phosphates, had a negative effect on alkali activation, as mentioned in earlier studies [62,63].

In this study, the PLR50MK50 AAM produced when the ratios SiO_2/Al_2O_3 and $(SiO_2 + Al_2O_3)/Na_2O$ in the reactive paste were 10% lower and 20% higher, respectively,

compared to the PLR70MK30 AAM, which acquired almost 40% higher compressive strength at 26 MPa.

3.4. Physical Properties of AAMs

Table 6 shows the physical properties of PLR50MK50 and PLR70MK30 AAMs produced under the optimum synthesis conditions. It is seen from these data that porosity, water absorption, and apparent density had quite similar values, which were the average ones of the three measurements taken. Thus, the difference in the compressive strength, which was almost 50%, was probably due to the presence of denser microstructures and specific mineralogical phases.

Table 6. Physical properties of selected AAMs [1].

AAMs Code	Compressive Strength (MPa)	Porosity (%)	Water Absorption (%)	Apparent Density (g cm^{-3})
PLR50MK50	25.9	7.0	4.2	1.7
PLR70MK30	17.6	7.3	4.5	1.6

[1] H_2O/Na_2O = 14.6, SiO_2/Na_2O = 1.0, curing at 40 °C for 24 h and ageing for 7 days.

3.5. Structural Integrity of PLR50MK50 AAMs

The structural integrity of the PLR50MK50 AAMs was evaluated through the implementation of different durability tests, including firing at 200, 500, and 800 °C for 2h, and immersion in distilled water and a 1 mol L^{-1} HCl solution for 7 days. Table 7 shows the compressive strength (MPa), weight loss (%) and volumetric shrinkage (%), as obtained after the implementation of each test.

Table 7. Selected properties of PLR50MK50 AAMs obtained from durability tests.

Durability Test	Period	Compressive Strength (MPa)	Weight Loss (%)	Shrinkage (%)
Control AAMs [1]	-	25.9	-	-
Firing at 200 °C	2 h	20.4	0.4	3.5
Firing at 500 °C	2 h	5.9	4.7	6.9
Immersion in H_2O	7 days	21.8	0.2	3.1
Immersion in 1M HCl	7 days	12.0	0.9	4.7

[1] H_2O/Na_2O = 14.6, SiO_2/Na_2O = 1.0, curing at 40 °C for 24 h and ageing for 7 days.

It is seen from these data that when the AAMs were fired at 200 °C, the compressive strength was reduced by almost 20% to 20.4 MPa. On the other hand, when higher firing temperatures were used, the specimens were severely damaged, due to phase transformations which deteriorated their structural integrity [64]. The compressive strength obtained after heating at 500 °C was only 5.9 MPa, while heating at 500 °C resulted in the formation of cracks and the almost complete destruction of the specimen. During heating between 130–160 °C, gypsum ($CaSO_4 \cdot 2H_2O$), which is a hydrated mineral shown in the XRD pattern of the PLR (Figure 3), was transformed first into hemihydrate ($CaSO_4 \cdot 0.5H_2O$) and then to anhydrite ($CaSO_4$), which was formed after heating at 290–900 °C [65]. Additional heating may have resulted in the partial decomposition of gypsum, the formation of CaO, and the deterioration of the structural stability of the specimens. It was mentioned that AAMs exhibiting much better structural integrity were produced from Greek laterite leaching residues, as a recent study indicated [37]. It is known that improved durability under firing at higher temperature is exhibited by AAMs produced from raw materials or by-products with much higher inherent alkali activation potential, such as slags or fly ashes. The thermostability and thermal insulation performance of the produced AAMs may have been further improved if the specimens were reinforced with fibers, or if the calcination of the raw materials took place prior to alkali activation [66–69].
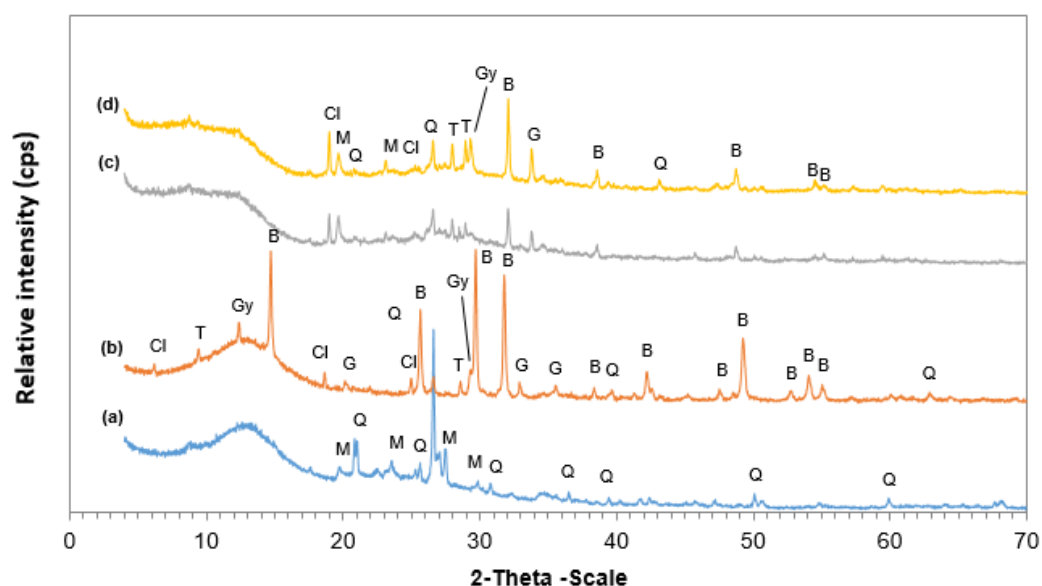
Figure 3. XRD patterns of (a) metakaolin (MK), (b) leaching residues PLR, (c) PLR50MK50, and (d) PLR70MK30 AAMs. Phases identified are: bassanite (B), calcite (C), clinochlore (Cl), goethite (G), gypsum (Gy), muscovite (M), quartz (Q), talc (T). The AAMs produced at 40 °C with the use of 10 M NaOH.

On the other hand, immersion of the AAMs in water for 7 days resulted in an almost 15% compressive strength loss (21.8 MPa), which increased by more than 50% (12 MPa) after the immersion of specimens for the same period in a much more aggressive 1 mol L^{-1} HCl solution. Weight loss and shrinkage were quite similar in all cases and varied between 0.4%–4.7% and 3.1%–6.9%, respectively.

3.6. Comparison with a Previous Study

The present study is the second one that attempts to explore the alkali activation potential of laterite leaching residues. The first one was carried out a year ago [37] and explored the potential for alkali activation of Greek laterite leaching residues (GLR) after mixing them with metakaolin (MK) at a mass ratio of GLR:MK 90:10. The synthesis conditions were: NaOH molarity of 8 M, curing temperature at 80 °C, curing period for 24 h and ageing period for 7 days. The main difference was that the curing temperature in the present study was lower, at 40 °C. Table 8 presents the experimental conditions and compares the results obtained from each of the two studies.

Table 8. Comparison of alkali activation of two laterite leaching residues.

Raw Materials		Greek Laterite Leaching Residues (GLR)	Polish Laterite Leaching Residues (PLR)
Chemical composition (wt%)	SiO_2	30.8	23.3
	Al_2O_3	2.3	1.2
	CaO	3.7	17.9
	SO_3	6.12	30.6
	Fe_2O_3	50.9	9.0
Reactivity (mg L^{-1})	Si	20.1	59.1
	Al	2.4	0.5
AAMs		GLR90MK10	PLR50MK50
Molar ratio in the activating solution	H_2O/Na_2O	17.4	14.6
	SiO_2/Na_2O	1	1
Molar ratio in the reactive paste	$(SiO_2 + Al_2O_3)/Na_2O$	9.3	5.1
	Fe_2O_3/CaO	4.8	0.2

Table 8. *Cont.*

Raw Materials	Greek Laterite Leaching Residues (GLR)	Polish Laterite Leaching Residues (PLR)
Curing Conditions	80 °C, 24 h, 7 days	40 °C, 24 h, 7 days
L/S ratio	0.3	0.6
Porosity (%)	21.3	7.0
Water Absorption (%)	5.1	4.2
Density (g cm^{-3})	2.3	1.7
Compressive strength (MPa)	41	26
References	[37]	This study

It is seen from these results that the GLR were more efficiently alkali activated because (i) the addition of metakaolin was very low, only 10 wt%, compared to 50 wt% used in the present study, and (ii) the compressive strength acquired was almost 50% higher (41 MPa) compared to the maximum value of the present study (26 MPa).

These differences are mainly due to the following reasons:

- The SiO_2 and Al_2O_3 content of the GLR were significantly higher (30.8 wt% SiO_2 and 2.3 wt% Al_2O_3), compared to the respective values of the PLR, namely 23.3 and 1.2 wt%.
- The Si and Al concentrations after the leaching of each residue with NaOH solution were 20.1 and 2.4 mg L^{-1}, respectively, for the GLR (when 8 M NaOH solution was used), compared to 59.1 and 0.5 mg L^{-1}, respectively, for the PLR (when 10 M NaOH solution was used); this indicated a deficiency of Al species in the solution in the second case, which was not favorable for the development of aluminosilicate bonds.
- The molar ratio $(SiO_2 + Al_2O_3)/Na_2O$ was more favorable in the reactive phase of the GLR.
- The PLR had a high content of sulfates (30.6 wt%), which were shown as SO_3 in Table 2 and confirmed by the presence of gypsum (Figure 3). Such sulfate compounds may have caused internal expansion during curing, ageing, and solidification [70]. The presence of gypsum in the precursors and its effect during alkali activation has been investigated in earlier studies, and the results varied. For example, Cong et al. [71] stated that silica fume could be used for the improvement of fly ash/slag-based geopolymers activated with calcium carbide residue and gypsum. On the other hand, exposure of specimens to 5% $MgSO_4$ resulted in the formation of gypsum and ettringite, which caused surface spalling, cracking and the deterioration of the structural integrity of one-part geopolymers [72]. In another study, prior to efficient valorization of sulfidic mine waste for the production of construction materials, the extraction of hazardous contaminants and the removal of sulfur using flotation or bioleaching was carried out [73].
- The content of the CaO in the PLR was much higher (17.9 wt%) compared to the respective one of the GLR (3.7 wt%), and this may have created implications during alkali activation. The role of CaO/Fe_2O_3 molar ratios needs to be further elucidated. So far, the few studies which were carried out to elucidate this ratio indicate that low CaO/Fe_xO_y molar ratios enhance the early kinetics and compressive strength of the produced specimens; in the present study, the CaO/Fe_2O_3 molar ratio was 1.99, which was four times higher than the ratio recorded in the previous study, at 0.48. [37,74,75].
- The L/S ratio in GLR was smaller and thus more suitable for the production of specimens with higher compressive strengths. This ratio varied for different materials, but played an important role in assessing the viscosity and flowability of the paste. In several cases, low L/S ratios resulted in the production of AAMs with more compact microstructures and beneficial properties [61,76].

3.7. Characterization of Selected AAMs

3.7.1. Mineralogical Analysis

Figure 3 presents the XRD patterns of raw materials, namely PLR and MK, as well as the XRD patterns of selected AAMs produced under the optimum synthesis conditions. It is seen that the AAMs consisted of quartz (SiO_2), talc [$Mg_3Si_4O_{10}(OH)_2$], muscovite

$[KAl_2(AlSi_3O_{10})(OH)_2]$, and clinochlore $[(Mg,Fe)_5Al(Si_3Al)O_{10}(OH)_8]$, which were phases also present in the raw materials. The PLR also contained bassanite and gypsum, which were phases formed during leaching through the reaction of H_2SO_4 with calcium carbonates present in the ore. The presence of calcium sulfates is also indicated in Table 2, which shows that the contents of CaO and SO_3 were 17.9 wt% and 30.6 wt%, respectively.

After alkali activation, it was observed that most bassanite peaks disappeared, while the intensities of most other peaks were substantially decreased as a result of reactions between the precursors and the highly alkaline activating solution. The patterns of the AAMs indicated a certain degree of amorphicity due to the presence of a shoulder between 2-Theta 20°–30° which was more clearly visible in pure MK-based AAMs [77,78]. Similar phases were also observed in the XRD patterns shown in earlier studies [31,37,79–81].

3.7.2. FTIR Analysis

Figure 4 shows the FTIR spectra, over the range 4000–400 cm^{-1}, of laterite leaching residues (PLR) and selected AAMs (PLR50MK50 and PLR70MK30) produced under the optimum synthesis conditions.
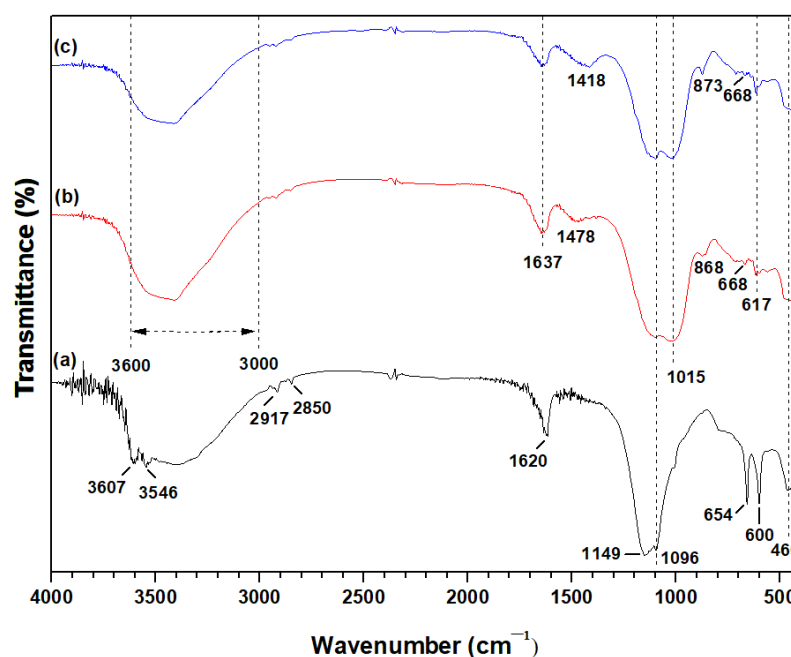

Figure 4. FTIR spectra of (a) leaching residues PLR, (b) PLR50MK50 and (c) PLR70MK30 AAMs.

The bands present in the PLR residues at 2850 cm^{-1} and 2917 cm^{-1} were assigned to hydrocarbon stretches, while the small bands at 3546 cm^{-1} and 3607 cm^{-1} were attributed to Fe^{3+}-OH-Fe^{3+} stretching and deformation vibrations. The band seen at 1096 cm^{-1} in PLR residues corresponded to asymmetric stretching vibrations of the silicate tetrahedral network. Furthermore, the bands shown at 1620 cm^{-1} in PLR residues and 1637 cm^{-1} in both AAMs were due to -OH bending vibrations [13]. The peak at 1149 cm^{-1} was associated with sulfate minerals, i.e., bassanite and gypsum [82]. This peak was clear in the PLR and less sharp in the produced AAMs, due to the partial reaction of the original gypsum with the alkaline solution and the development of amorphous phases [83]. The two bands shown at 600 and 654 cm^{-1} in the PLR residues could be assigned to the formation of calcium-based sulfates, as also indicated by the XRD pattern [37].

The band region between 3600 cm^{-1} and 3000 cm^{-1} in both AAMs was related to the stretching (-OH) and bending (H-O-H) vibrations, due to the hydration processes that took place during alkali activation [84].

The board bands detected at ~1478 cm^{-1} in the PLR50MK50 AAM (Figure 4b) and ~1418 cm^{-1} in the PLR70MK30 AAM (Figure 4c) were associated with the asymmetric

stretching vibrations of O-C-O bonds and indicated the formation of carbonation products from the reaction of alkali-activated silicates with atmospheric CO_2 during the curing period [34]. The band at 1015 cm^{-1} in both AAMs was attributed to Si-O-Si, Fe-O-Si and Si-O-Al stretching vibrations of the growing inorganic polymer network [18]. The small bands at 868 cm^{-1} and 873 cm^{-1}, shown in the AAMs were due to the out-of-plane bending vibrations of the carbonate ions [34]. The bands in the region 600 and 800 cm^{-1} shown in both AAMs (Figure 4b,c) were related to Si-O-Al deformation vibrations [85]. The characteristic band of quartz at 460 cm^{-1} remained unaffected in both AAMs, due to the low reactivity of this mineral phase in alkaline systems, as also indicated in a previous recent study [37].

3.7.3. SEM Analysis

Figures 5 and 6 show SEM-back-scattered electron (BSE) images of the PLR and selected AAMs (PLR50MK50 and PLR70MK30) produced under optimum conditions, respectively. The PLR consist of small and inter-grown particles that eventually form spherically aggregated precipitates (Figure 5a). In agreement with the XRD results, the dominant presence of well-defined crystals of bassanite and gypsum was identified on the free surface of the PLR and is shown in detail in Figure 5b (zoom of rectangular area of Figure 5a). Previous studies have confirmed the co-existence of calcium sulphate precipitates with different degrees of hydration in laterite leaching residues, including bassanite ($CaSO_4 \cdot 0.5H_2O$), gypsum ($CaSO_4 \cdot 2H_2O$), and anhydrite ($CaSO_4$), due to attack from the acidic solution [86,87].
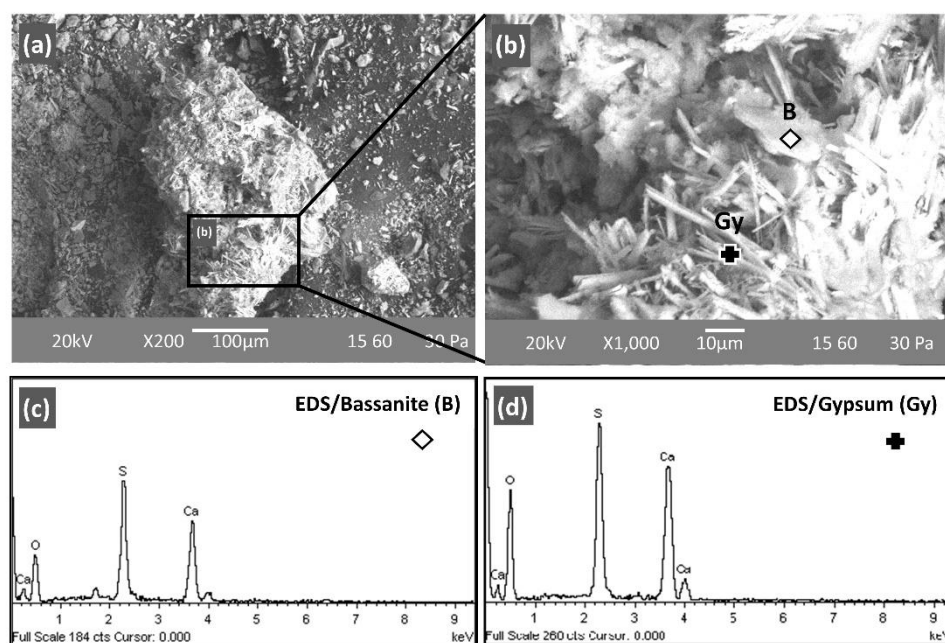

Figure 5. SEM-back-scattered electron (SEM-BSE) images of Polish laterite leaching residues (PLR) at several magnifications i.e., (**a**) ×200 and (**b**) ×1000. Energy dispersive X-ray spectroscopy (EDS) spectra at 1000 indicated the presence of (**c**) bassanite and (**d**) gypsum in the form of rosettes and prismatic crystals, respectively.
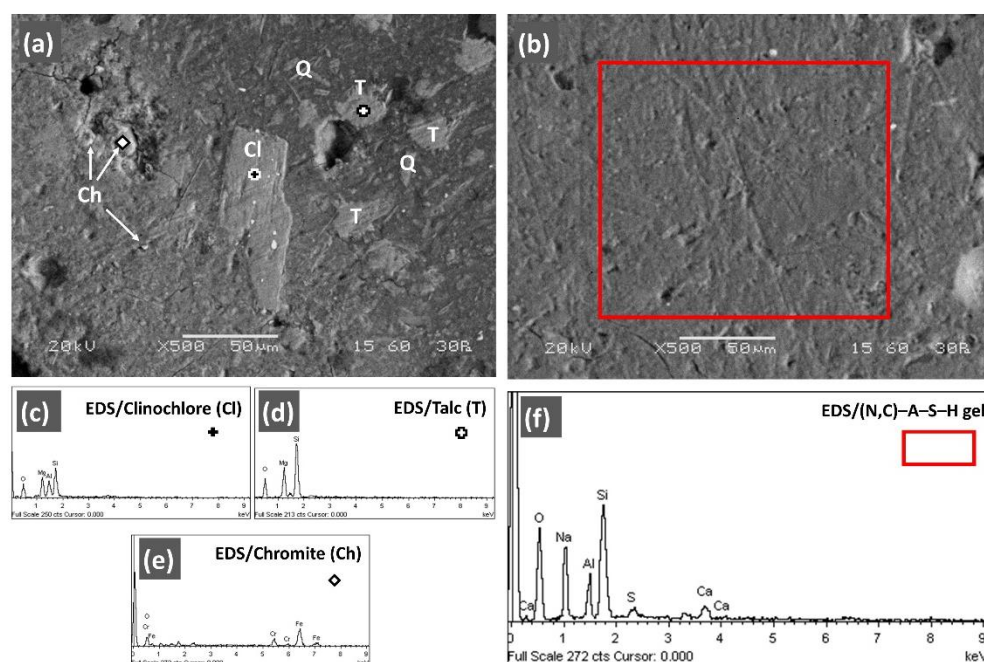
Figure 6. Cross-sectional SEM images of selected AAMs produced by mixing Polish laterite leaching residues (PLR) and metakaolin (MK) at mass ratio (**a**) 70:30 (PLR70MK30) and (**b**). 50:50 (PLR50MK50). EDS spectra showed in several spot locations (**c–e**) and (**f**) areas (red rectangle) the presence of undissolved oxide phases and newly formed inorganic gels [Cl: Clinochlore, T: Talc, Q: Quartz, Ch: chromite, Gel: (N,C)–A–S–H].

Among the examined AAMs, significant differences in the microstructure and the alkali-activation reaction products were observed in cross-sections, depending on the mixing ratios of the precursors/binders used. In this context, the SEM/EDS examination of PLR70MK30 AAM (Figure 6a) revealed a heterogeneous structure with an adequate cohesion between the paste and the PLR. As shown in the XRD patterns, this microstructure was dominated by large clinochlore [$(Mg,Fe)_5Al(Si_3Al)O_{10}(OH)_8$] crystals (>50 μm) along with several smaller crystals (<20 μm) of talc [$Mg_3Si_4O_{10}(OH)_2$] and some grains of chromite ($FeCr_2O_4$). The observation of several unreacted and/or partially dissolved particles, as well as hollow cavities and microcracks in the inorganic matrix of the PLR50MK30 AAM, may have decreased its durability, and this was confirmed by the lower compressive strength (17.6 MPa) obtained for this specimen compared to the PLR50MK50 AAM (25.9 MPa). As shown in Figure 5b, the PLR50MK50 AAM exhibited a denser and more compact microstructure, with strong bonding with the inorganic matrix and almost no presence of voids or unreacted particles, when compared to PLR70MK30 AAM, which justifies its higher durability. SEM-EDS analyses, carried out in cross-sectional areas of the PLR50MK50 AAM, confirmed the compact and homogenous formation of (N,C)–A–S–H polymeric gel with high ratios of Na/Si and Al/Si, at 0.51 and 0.33, respectively; on the other hand, the gel was poor in calcium (Ca/Si ratio of 0.08) and sulfur/sulfates (S/Si ratio of 0.02). This low content of calcium sulphate-hydrated phases (bassanite and gypsum) inside the polymeric network of the PLR50MK50 AAM indicated the synergistic interaction between the metakaolin added in the starting mixture at a 50:50 ratio and the alkaline activators (NaOH and Na_2SiO_3 solutions), which resulted in their extensive dissolution in the polymeric matrix [37].

3.8. Toxicity Assessment

Table 9 shows the toxicity of the PLR and the PLR50MK50 AAM after the application of the EN 12457-3 test.

Table 9. EN 12457-3 results (L/S = 10 L kg^{-1}).

Elements	Raw Material	AAMs	Limit Values *		
	Leaching Residues (PLR)	PLR50MK50	For Wastes Accepted at Landfills for Inert Wastes	For Non Hazardous Wastes	For Wastes Accepted at Landfills for Hazardous Wastes
	mg kg^{-1}				
Al	5.4	15.7	-	-	-
Cr	0.3	0.3	0.5	10	50
Mn	98.2	0.2	-	-	-
Fe	7.3	29.8	-	-	-
Ni	449.4	0.6	0.4	10	40
Cu	0.3	0.06	2	50	100
Zn	3.9	0.4	4	50	200
As	<DL	0.06	0.5	2	25
Mo	0.7	0.05	0.5	10	30
Cd	0.4		0.04	1	5
Pb	0.6	0.01	0.5	10	50
SO$_4^{2-}$	800	80	1000	20,000	50,000

* Council Decision 2003/33/EC.

It is seen that the toxicity of the PLR far exceeded the limits given for all disposal options except for Ni, which exhibited a dissolution rate of 449.4 mg kg^{-1}; thus, they could not be disposed of in any landfill without treatment. The determined dissolution rate of Zn (3.9 mg kg^{-1}) was almost equal to the limit (4.0 mg kg^{-1}) for landfills accepting inert wastes. Increased dissolution rates were also observed for the sulphate ions of the PLR, but the values determined were definitely below all limits. The PLR50MK50 AAM exhibited extremely low toxicity, except for Ni, which exhibited a dissolution rates of 0.6 mg kg^{-1}, which slightly exceeded the limit set for wastes accepted at landfills for inert wastes.

Based on these results, the alkali activation of laterite leaching residues with the addition of metakaolin resulted in the production of AAMs with very low toxicity; the only element that marginally exceeded the lower limits was Ni. It is believed that if the PLR is co-alkali activated with other wastes, including for example metallurgical slags or construction and demolition wastes, the toxicity of the produced AAMs will be minimized as seen in previous relevant studies [21,49].

4. Conclusions

Laterite leaching residues, obtained after the sulfuric acid leaching of Polish ores in stirred reactors under atmospheric conditions, exhibited very low inherent alkali activation potential. However, they could be efficiently alkali activated at a low temperature, of 40 °C, if mixed with metakaolin at the mass ratio of 50:50, and the obtained compressive strength of the specimens after an ageing period of 7 days reached 26 MPa. This was mainly due to the pozzolanic nature of metakaolin and the adjustment of the Si:Al ratio in the reactive paste. The molar ratios which were important in the activating solution and defined the efficiency of alkali activation were H$_2$O/Na$_2$O and H$_2$O/Na$_2$O.

The structural integrity of the produced AAMs was acceptable. When the specimens were fired for one hour at 200 °C, the compressive strength was reduced by almost 20%. When higher firing temperature was used, phase transformations took place, which deteriorated their structural integrity, and the compressive strength was reduced substantially to almost 6 MPa. On the other hand, the immersion of AAMs in water for 7 days resulted in an almost 20% reduction in compressive strength, which exceeded 50% when a more aggressive HCl solution was used.

The microstructure of selected AAMs, produced after the mixing of PLR and MK at equal mass ratios using SEM/EDS, was homogeneous, compact, and revealed the formation of a strong (N,C)–A–S–H polymeric gel, which eventually improved the mechanical properties.

The produced AAMs exhibited very low toxicity, as indicated by the application of the EN 12457-3 test, while the only element that slightly exceeded the limits for wastes accepted at landfills for inert wastes was nickel.

Overall, the results of this study indicate that alkali activation can be a viable option for the valorization of laterite leaching residues and the production of AAMs with beneficial properties that can be used as binders or construction materials. Future studies will involve the co-valorization of leaching residues with metallurgical slags or construction and demolition wastes in line with circular economy principles. This approach will definitely contribute to reduction of the footprints of several industrial processes. The role of gypsum or other sulfides or sulfates present in the initial wastes during alkali activation will be also further investigated.

Author Contributions: Conceptualization, K.K.; methodology, K.K. and V.K.; validation, V.K., E.P. and G.B.; investigation, V.K.; data curation, V.K., E.P. and G.B.; writing—original draft preparation, V.K., E.P. and G.B.; writing—review and editing, K.K.; project administration, K.K. All authors have read and agreed to the published version of the manuscript.

Data Availability Statement: Not applicable.

Conflicts of Interest: The authors declare no conflict of interest.

References

1. Obonyo, E.A.; Kamseu, E.; Lemougna, P.N.; Tchamba, A.B.; Melo, U.C.; Leonelli, C. Sustainable Approach for the Geopolymerization of Natural Iron-Rich Aluminosilicate Materials. *Sustainability* **2014**, *6*, 5535–5553. [CrossRef]
2. Kamseu, E.; Kaze, C.R.; Fekoua, J.N.N.; Melo, U.C.; Rossignol, S.; Leonelli, C. Ferrisilicates formation during the geopolymerization of natural Fe-rich aluminosilicate precursors. *Mater. Chem. Phys.* **2020**, *240*, 122062. [CrossRef]
3. Henne, A.; Craw, D.; Gagen, E.J.; Southam, G. Contribution of bacterially-induced oxidation of Fe-silicates in iron-rich ore to laterite formation, Salobo IOCG mine, Brazil. *Chem. Geol.* **2020**, *539*, 119499. [CrossRef]
4. Favier, S.; Teitler, Y.; Golfier, F.; Cathelineau, M. Multiscale physical–chemical analysis of the impact of fracture networks on weathering: Application to nickel redistribution in the formation of Ni-laterite ores, New Caledonia. *Ore Geol. Rev.* **2022**, *147*, 104971. [CrossRef]
5. Zhang, P.; Guo, Q.; Wei, G.; Meng, L.; Han, L.; Qu, J.; Qi, T. Extraction of metals from saprolitic laterite ore through pressure hydrochloric-acid selective leaching. *Hydrometallurgy* **2015**, *157*, 149–158. [CrossRef]
6. Zhou, Z.; Ma, B.; Wang, C.; Chen, Y.; Wang, L. Separation and recovery of scandium from high pressure sulfuric acid leach liquor of limonitic laterite. *Process Saf. Environ.* **2022**, *165*, 161–172. [CrossRef]
7. McDonald, R.G.; Whittington, B.I. Atmospheric acid leaching of nickel laterites review: Part I. Sulphuric acid technologies. *Hydrometallurgy* **2008**, *91*, 35–55. [CrossRef]
8. Khoo, J.Z.; Haque, N.; Woodbridge, G.; McDonald, R.; Bhattacharya, S. A life cycle assessment of a new laterite processing technology. *J. Clean. Prod.* **2017**, *142*, 1765–1777. [CrossRef]
9. Mystrioti, C.; Papassiopi, N.; Xenidis, A.; Komnitsas, K. Counter-Current Leaching of Low-Grade Laterites with Hydrochloric Acid and Proposed Purification Options of Pregnant Solution. *Minerals* **2018**, *8*, 599. [CrossRef]
10. Tian, Q.; Dong, B.; Guo, X.; Xu, Z.; Wang, Q.; Li, D.; Yu, D. Comparative atmospheric leaching characteristics of scandium in two different types of laterite nickel ore from Indonesia. *Miner. Eng.* **2021**, *173*, 107212. [CrossRef]
11. Agatzini-Leonardou, S.; Tsakiridis, P.E.; Oustadakis, P.; Karidakis, T.; Katsiapi, A. Hydrometallurgical process for the separation and recovery of nickel from sulphate heap leach liquor of nickeliferrous laterite ores. *Miner. Eng.* **2009**, *22*, 1181–1192. [CrossRef]
12. Quast, K.; Xu, D.; Skinner, W.; Nosrati, A.; Hilder, T.; Robinson, D.J.; Addai-Mensah, J. Column leaching of nickel laterite agglomerates: Effect of feed size. *Hydrometallurgy* **2013**, *134–135*, 144–149. [CrossRef]
13. Komnitsas, K.; Petrakis, E.; Pantelaki, O.; Kritikaki, A. Column Leaching of Greek Low-Grade Limonitic Laterites. *Minerals* **2018**, *8*, 377. [CrossRef]
14. Komnitsas, K.; Zaharaki, D. Geopolymerisation: A review and prospects for the minerals industry. *Miner. Eng.* **2007**, *20*, 1261–1277. [CrossRef]
15. Krivenko, P.V.; Kovalchuk, G.Y. Directed synthesis of alkaline aluminosilicate minerals in a geocement matrix. *J. Mater. Sci.* **2007**, *42*, 2944–2952. [CrossRef]

16. Kamseu, E.; Rizzuti, A.; Leonelli, C.; Perera, D. Enhanced thermal stability in K_2O Metakaolin-Based geopolymer concretes by Al_2O_3 and SiO_2 fillers addition. *J. Mater. Sci.* **2010**, *45*, 1715–1724. [CrossRef]

17. Kamseu, E.; Nait-Ali, B.; Bignozzi, M.C.; Leonelli, C.; Rossignol, S.; Smith, D.S. Bulk composition and microstructure dependence of effective thermal conductivity of porous inorganic polymer cements. *J. Eur. Ceram. Soc.* **2012**, *32*, 1593–1603. [CrossRef]

18. Kaze, R.C.; Beleukà Moungam, L.M.; Fonkwe Djouka, M.L.; Nana, A.; Kamseu, E.; Chinje Melo, U.F.; Leonelli, C. The corrosion of kaolinite by iron minerals and the effects on geopolymerization. *Appl. Clay Sci.* **2017**, *138*, 48–62. [CrossRef]

19. Martin, A.; Pastor, J.Y.; Palomo, A.; Fernández-Jiménez, A. Mechanical behaviour at high temperature of alkali-activated aluminosilicates (geopolymers). *Constr. Build. Mater.* **2015**, *93*, 1188–1196. [CrossRef]

20. Komnitsas, K.; Zaharaki, D.; Vlachou, A.; Bartzas, G.; Galetakis, M. Effect of synthesis parameters on the quality of construction and demolition wastes (CDW) geopolymers. *Adv. Powder Technol.* **2015**, *26*, 368–376. [CrossRef]

21. Komnitsas, K.; Yurramendi, L.; Bartzas, G.; Karmali, V.; Petrakis, E. Factors affecting co-valorization of fayalitic and ferronickel slags for the production of alkali activated materials. *Sci. Total Environ.* **2020**, *721*, 137753. [CrossRef] [PubMed]

22. Mehta, A.; Siddique, R. Sustainable geopolymer concrete using ground granulated blast furnace slag and rice husk ash: Strength and permeability properties. *J. Clean. Prod.* **2018**, *205*, 49–57. [CrossRef]

23. Davidovits, J. Geopolymers—Inorganic polymeric new materials. *J. Therm. Anal. Calorim.* **1991**, *37*, 1633–1656. [CrossRef]

24. Khale, D.; Chaudhary, R. Mechanism of geopolymerization and factors influencing its development: A review. *J. Mater. Sci.* **2007**, *42*, 729–746. [CrossRef]

25. Bernal, S.A.; de Gutierrez, R.M.; Provis, J.L.; Rose, V. Effect of silicate modulus and metakaolin incorporation on the carbonation of alkali silicate-activated slags. *Cem. Concr. Res.* **2010**, *40*, 898–907. [CrossRef]

26. Peys, A.; Douvalis, A.P.; Siakati, C.; Rahier, H.; Blanpain, B.; Pontikes, Y. The influence of air and temperature on the reaction mechanism and molecular structure of Fe-silicate inorganic polymers. *J. Non-Cryst. Solids* **2019**, *526*, 119675. [CrossRef]

27. Soultana, A.; Valouma, A.; Bartzas, G.; Komnitsas, K. Properties of Inorganic Polymers Produced from Brick Waste and Metallurgical Slag. *Minerals* **2019**, *9*, 551. [CrossRef]

28. Traven, K.; Češnovar, M.; Ducman, V. Particle size manipulation as an influential parameter in the development of mechanical properties in electric arc furnace slag-based AAM. *Ceram. Int.* **2019**, *45*, 22632–22641. [CrossRef]

29. Komnitsas, K.; Zaharaki, D.; Perdikatsis, V. Effect of synthesis parameters on the compressive strength of low-calcium ferronickel slag inorganic polymers. *J. Hazard. Mater.* **2009**, *161*, 760–768. [CrossRef]

30. Lemougna, P.N.; Madi, A.B.; Kamseu, E.; Melo, U.C.; Delplancke, M.-P.; Rahier, H. Influence of the processing temperature on the compressive strength of Na activated lateritic soil for building applications. *Constr. Build. Mater.* **2014**, *65*, 60–66. [CrossRef]

31. Lemougna, P.N.; Wang, K.-T.; Tang, Q.; Kamseu, E.; Billong, N.; Melo, U.C.; Cui, X.-M. Effect of slag and calcium carbonate addition on the development of geopolymer from indurated laterite. *Appl. Clay Sci.* **2017**, *148*, 109–117. [CrossRef]

32. Gualtieri, M.L.; Romagnoli, M.; Pollastri, S.; Gualtieri, A.F. Inorganic polymers from laterite using activation with phosphoric acid and alkaline sodium silicate solution: Mechanical and microstructural properties. *Cem. Concr. Res.* **2015**, *67*, 259–270. [CrossRef]

33. Kaze, R.C.; Beleukà Moungam, L.M.; Cannio, M.; Rosa, R.; Kamseu, E.; Melo, U.C.; Leonelli, C. Microstructure and engineering properties of $Fe_2O_3(FeO)$-Al_2O_3-SiO_2 based geopolymer composite. *J. Clean. Prod.* **2018**, *199*, 849–859. [CrossRef]

34. Kaze, C.R.; Venyite, P.; Nana, A.; Juvenal, D.N.; Tchakoute, H.K.; Rahier, H.; Kamseu, E.; Melo, U.C.; Leonelli, C. Meta-halloysite to improve compactness in iron-rich laterite-based alkali activated materials. *Mater. Chem. Phys.* **2020**, *239*, 122268. [CrossRef]

35. Komnitsas, K.; Petrakis, E.; Bartzas, G.; Karmali, V. Column leaching of low-grade saprolitic laterites and valorization of leaching residues. *Sci. Total Environ.* **2019**, *665*, 347–357. [CrossRef] [PubMed]

36. Kaze, R.C.; Naghizadeh, A.; Tchadjie, L.; Adesina, A.; Djobo, J.N.Y.; Nemaleu, J.G.D.; Kamseu, E.; Melo, U.C.; Tayeh, B.A. Lateritic soils based geopolymer materials: A review. *Constr. Build. Mater.* **2022**, *344*, 128157. [CrossRef]

37. Komnitsas, K.; Bartzas, G.; Karmali, V.; Petrakis, E. Factors Affecting Alkali Activation of Laterite Acid Leaching Residues. *Environments* **2021**, *8*, 4. [CrossRef]

38. Gharzouni, A.; Sobrados, I.; Joussein, E.; Baklouti, S.; Rossignol, S. Predictive tools to control the structure and the properties of metakaolin based geopolymer materials. *Colloids Surf. A* **2016**, *511*, 212–221. [CrossRef]

39. Wang, R.; Wang, J.; Dong, T.; Ouyang, G. Structural and mechanical properties of geopolymers made of aluminosilicate powder with different $SiO_2/Al2O_3$ ratio: Molecular dynamics simulation and microstructural experimental study. *Constr. Build. Mater.* **2020**, *240*, 117935. [CrossRef]

40. *NP EN 1936:2006*; Natural Stone Test Methods—Determination of Real Density and Apparent Density and of Total and Open Porosity. British Standards Institute: London, UK, 2007.

41. *BS EN 12457-3:2002*; Characterisation of Waste—Leaching—In Compliance Test for Leaching of Granular Waste Materials and Sludges. Two Stage Batch Test at a Liquid to Solid Ratio of 2 L/kg and 8 L/kg for Materials with a High Solid Content and with a Particle Size below 4 mm (without or with Size Reduction). British Standards Institute: London, UK, 2002.

42. Van der Sloot, H.A.; Hjelmar, O.; Bjerre Hansen, J.; Woitke, P.; Lepom, P.; Leschber, R.; Bartet, B.; Debrucker, N. *Validation of CEN/TC 292 Leaching Tests and Eluate Analysis Methods prEN 12457 1-4, ENV 13370 and ENV 12506 in Co-Operation with CEN/TC 308*; ECN: Petten, The Netherlands, 2001; Available online: https://publicaties.ecn.nl/PdfFetch.aspx?nr=ECN-C--01-117 (accessed on 9 November 2018).

43. *Council Decision 2003/33/EC*; Establishing Criteria and Procedures for the Acceptance of Waste at Landfills Pursuant to Article16 of and Annex II to Directive 1999/31/EC. European Commission: Brussels, Belgium, 2003. Available online: https://eur-lex.europa.eu/legal-content/EN/TXT/PDF/?uri=CELEX:32003D0033&qid=1669176321070&from=EN (accessed on 15 June 2022).

44. Bumanis, G.; Vitola, L.; Bajare, D.; Dembovska, L.; Pundiene, I. Impact of reactive SiO_2/Al_2O_3 ratio in precursor on durability of porous alkali activated materials. *Ceram. Int.* **2017**, *43*, 5471–5477. [CrossRef]

45. Juengsuwattananon, K.; Winnefeld, F.; Chindaprasirt, P.; Pimraksa, K. Correlation between initial SiO_2/Al_2O_3, Na_2O/Al_2O_3, Na_2O/SiO_2 and H_2O/Na_2O ratios on phase and microstructure of reaction products of metakaolin-rice husk ash geopolymer. *Constr. Build. Mater.* **2019**, *226*, 406–417. [CrossRef]

46. Hertel, T.; Pontikes, Y. Geopolymers, inorganic polymers, alkali-activated materials and hybrid binders from bauxite residue (red mud)–Putting things in perspective. *J. Clean. Prod.* **2020**, *258*, 120610. [CrossRef]

47. He, P.; Wang, M.; Fu, S.; Jia, D.; Yan, S.; Yuan, J.; Xu, J.; Wang, P.; Zhou, Y. Effects of Si/Al ratio on the structure and properties of metakaolin based geopolymer. *Ceram. Int.* **2016**, *42*, 14416–14422. [CrossRef]

48. Gado, R.A.; Hebda, M.; Łach, M.; Mikuła, J. Alkali Activation of Waste Clay Bricks: Influence of The Silica Modulus, SiO_2/Na_2O, H_2O/Na_2O Molar Ratio, and Liquid/Solid Ratio. *Materials* **2020**, *13*, 383. [CrossRef] [PubMed]

49. Komnitsas, K.; Bartzas, G.; Karmali, V.; Petrakis, E.; Kurylak, W.; Pietek, G.; Kanasiewics, J. Assessment of alkali activation potential of a Polish ferronickel slag. *Sustainability* **2019**, *11*, 1863. [CrossRef]

50. Mo, L.; Zhang, F.; Deng, M.; Jin, F.; Al-Tabbaa, A.; Wang, A. Accelerated carbonation and performance of concrete made with steel slag as binding materials and aggregates. *Cem. Concr. Compos.* **2017**, *83*, 138–145. [CrossRef]

51. Gebregziabiher, B.S.; Thomas, R.J.; Peethamparan, S. Temperature and activator effect on early-age reaction kinetics of alkali-activated slag binders. *Constr. Build. Mater.* **2016**, *113*, 783–793. [CrossRef]

52. Yuan, J.; He, P.; Jia, D.; Yang, C.; Zhang, Y.; Yan, S.; Yang, Z.; Duan, X.; Wang, S.; Zhou, Y. Effect of curing temperature and SiO_2/K_2O molar ratio on the performance of metakaolin-based geopolymers. *Ceram. Int.* **2016**, *42*, 16184–16190. [CrossRef]

53. Komnitsas, K. Co-valorization of marine sediments and construction & demolition wastes through alkali activation. *J. Environ. Chem. Eng.* **2016**, *4*, 4661–4669. [CrossRef]

54. Zaharaki, D.; Galetakis, M.; Komnitsas, K. Valorization of construction and demolition (C&D) and industrial wastes through alkali activation. *Constr. Build. Mater.* **2016**, *121*, 686–693. [CrossRef]

55. Chen, T.-A. Mechanical Properties of Glass-Based Geopolymers Affected by Activator and Curing Conditions under Optimal Aging Conditions. *Crystals* **2021**, *11*, 502. [CrossRef]

56. Falah, M.; Obenaus–Emler, R.; Kinnunen, P.; Illikainen, M. Effects of Activator Properties and Curing Conditions on Alkali-Activation of Low-Alumina Mine Tailings. *Waste Biomass Valorization* **2019**, *11*, 5027–5039. [CrossRef]

57. Provis, J.L.; Yong, C.Z.; Duxson, P.; van Deventer, J.S.J. Correlating mechanical and thermal properties of sodium silicate-fly ash geopolymers. *Colloids Surf. A* **2009**, *336*, 57–63. [CrossRef]

58. Clausi, M.; Fernández-Jiménez, A.M.; Palomo, A.; Tarantino, S.C.; Zenna, M. Reuse of waste sandstone sludge via alkali activation in matrices of fly ash and metakaolin. *Constr. Build. Mater.* **2018**, *172*, 212–223. [CrossRef]

59. Rakhimova, N.R.; Rakhimov, R.Z.; Morozov, V.P.; Gaifullin, A.R.; Potapova, L.I.; Gubaidullina, A.M.; Osin, Y.N. Marl-based geopolymers incorporated with limestone: A feasibility study. *J. Non Cryst. Solids* **2018**, *492*, 1–10. [CrossRef]

60. Tuyan, M.; Andiç-Çakir, Ö.; Ramyar, K. Effect of alkali activator concentration and curing condition on strength and microstructure of waste clay brick powder-based geopolymer. *Compos. Part B Eng.* **2018**, *135*, 242–252. [CrossRef]

61. Leong, H.Y.; Ong, D.E.L.; Sanjayan, J.G.; Nazari, A. The effect of different Na_2O and K_2O ratios of alkali activator on compressive strength of fly ash based-geopolymer. *Constr. Build. Mater.* **2016**, *106*, 500–511. [CrossRef]

62. Criado, M.; Fernández Jiménez, A.; Palomo, A. Effect of sodium sulfate on the alkali activation of fly ash. *Cement Concrete Compos.* **2010**, *32*, 589–594. [CrossRef]

63. Komnitsas, K.; Zaharaki, D.; Bartzas, G. Effect of sulphate and nitrate anions on heavy metal immobilisation in ferronickel slag geopolymers. *Appl. Clay Sci.* **2013**, *73*, 103–109. [CrossRef]

64. Zaharaki, D.; Komnitsas, K.; Perdikatsis, V. Use of analytical techniques for identification of inorganic polymer gel composition. *J. Mater. Sci.* **2010**, *45*, 2715–2724. [CrossRef]

65. Féjean, J.; Lanos, C.; Mélinge, Y.; Baux, C. Bahaviour of fire proofing materials containing gypsum, modifications induced by incorporation of inert filler. *Chem. Eng. Res. Des.* **2003**, *81*, 1230–1236. [CrossRef]

66. Wang, Z.; Wang, K.; Zhao, J.; Wang, S.; Shumuye, E.D.; Yang, Z. The mechanical properties of GFRP bars embedded in geopolymer concrete after high temperature exposure. *J. Build. Eng.* **2022**, *62*, 105355. [CrossRef]

67. Shumuye, E.D.; Zhao, J.; Wang, Z. Effect of the Curing Condition and High-Temperature Exposure on Ground-Granulated Blast-Furnace Slag Cement Concrete. *Int. J. Concr. Struct. Mater.* **2021**, *15*, 15. [CrossRef]

68. Majumder, A.; Stochino, F.; Farina, I.; Valdes, M.; Fraternali, F.; Martinelli, E. Physical and mechanical characteristics of raw jute fibers, threads and diatons. *Constr. Build. Mater.* **2022**, *326*, 126903. [CrossRef]

69. Kaze, C.R.; Lemougna, P.N.; Alomayri, T.; Assaedi, H.; Adesina, A.; Das, S.K.; Lecomte-Nana, G.-L.; Kamseu, E.; Melo, U.C.; Leonelli, C. Characterization and performance evaluation of laterite based geopolymer binder cured at different temperatures. *Constr. Build. Mater.* **2021**, *270*, 121443. [CrossRef]

70. Lee, L.; Lee, T.; Choi, H.; Lee, D.-E. Assessment of Optimum CaO Content Range for High Volume FA Based Concrete Considering Durability Properties. *Appl. Sci.* **2020**, *10*, 6944. [CrossRef]

71. Cong, P.; Mei, L. Using silica fume for improvement of fly ash/slag based geopolymer activated with calcium carbide residue and gypsum. *Constr. Build. Mater.* **2021**, *15*, 122171. [CrossRef]

72. Yang, T.; Gao, X.; Zhang, J.; Zhuang, X.; Wang, H.; Zhang, Z. Sulphate resistance of one-part geopolymer synthesized by calcium carbide residue-sodium carbonate-activation of slag. *Compos. Part B-Eng.* **2022**, *242*, 110024. [CrossRef]

73. Helser, J.; Perumal, P.; Cappuyns, V. Valorizing (cleaned) sulfidic mine waste as a resource for construction materials. *J. Environ. Manag.* **2022**, *319*, 115742. [CrossRef]

74. Peys, A.; White, C.E.; Rahier, H.; Blanpain, B.; Pontikes, Y. Alkali-activation of CaO-FeOx-SiO₂ slag. Formation mechanism from in-situ X-ray total scattering. *Cem. Concr. Res.* **2019**, *122*, 179–188. [CrossRef]

75. Siakati, C.; Douvalis, A.P.; Hallet, V.; Peys, A.; Pontikes, Y. Influence of CaO/FeO ratio on the formation mechanism and properties of alkali-activated Fe-rich slag. *Cem. Concr. Res.* **2021**, *146*, 146466. [CrossRef]

76. Jaya, N.A.; Liew, Y.M.; Heah, C.Y.; Abdullah, M.M.A.B. Effect of solid-to-liquid ratios on metakaolin geopolymers. In Proceedings of the 4th Electronic and Green Materials International Conference 2018 (EGM 2018), Bandung, Indonesia, 27–28 July 2018. [CrossRef]

77. Mahmoodi, O.; Siad, H.; Lachemi, M.; Dadsetan, S.; Sahmaran, M. Development of normal and very high strength geopolymer binders based on concrete waste at ambient environment. *J. Clean. Prod.* **2020**, *279*, 123436. [CrossRef]

78. Yi, C.; Boluk, Y.; Bindiganavile, V. Enhancing alkali-activation of metakaolin-based geopolymers using dry water. *J. Clean. Prod.* **2020**, *258*, 120676. [CrossRef]

79. Chen, I.A.; Hargis, C.W.; Juenger, M.C.G. Understanding expansion in calcium sulfoaluminate-belite cements. *Cem. Concr. Res.* **2012**, *42*, 51–60. [CrossRef]

80. García–Maté, M.; De la Torre, A.G.; León-Reina, L.; Losilla, E.R.; Aranda, M.A.G.; Santacruz, I. Effect of calcium sulfate source on the hydration of calcium sulfoaluminate eco-cement. *Cem. Concr. Compos.* **2015**, *55*, 53–61. [CrossRef]

81. Komnitsas, K.; Soultana, A.; Bartzas, G. Marble Waste Valorization through Alkali Activation. *Minerals* **2021**, *11*, 46. [CrossRef]

82. Bishop, J.L.; Lane, M.D.; Dyar, M.D.; King, S.J.; Brown, A.J.; Swayze, G.A. What lurks in the martian rocks and soil? Investigations of sulfates, phosphates, and perchlorates. Spectral properties of Ca-sulfates: Gypsum, bassanite, and anhydrite. *Am. Mineral.* **2014**, *99*, 2105–21151. [CrossRef]

83. Moreno-Maroto, J.M.; Delgado-Plana, P.; Cabezas-Rodríguez, R.; de Gutiérrez, R.M.; Eliche-Quesada, D.; Pérez-Villarejo, L.; Galán-Arboledas, R.J.; Bueno, S. Alkaline activation of high-crystalline low-Al₂O₃ Construction and Demolition Wastes to obtain geopolymers. *J. Clean. Prod.* **2022**, *330*, 129770. [CrossRef]

84. Adesanya, E.; Ohenoja, K.; Yliniemi, J.; Illikainen, M. Mechanical transformation of phyllite mineralogy toward its use as alkali-activated binder precursor. *Miner. Eng.* **2020**, *145*, 106093. [CrossRef]

85. Ricciotti, L.; Molino, A.J.; Roviello, V.; Chianese, E.; Cennamo, P.; Roviello, G. Geopolymer Composites for Potential Applications in Cultural Heritage. *Environments* **2017**, *4*, 91. [CrossRef]

86. Azimi, G.; Papangelakis, V.G. The solubility of gypsum and anhydrite in simulated laterite pressure acid leach solutions up to 250 °C. *Hydrometallurgy* **2010**, *102*, 1–13. [CrossRef]

87. da Silva, M.F.; de Sousa Oliveira, M.R.; dos Santos, I.D.; Radino-Rouse, R.; Mansur, M.B. Iron Precipitation Strategies from Nickel Laterite Ore Sulfuric Acid Leach Liquor. *Miner. Process. Extr. Met. Rev.* **2022**, *43*, 28–39. [CrossRef]